Characterization of the Fracture Properties of Aragonite- and Calcite-Filled Poly(ε-Caprolactone) by the Essential Work of Fracture Method

Ferenc Tuba,[1] László Oláh,[2] Péter Nagy[1]

[1]*Department of Polymer Engineering, Faculty of Mechanical Engineering, Budapest University of Technology and Economics, Müegyetem Rakpart 3, Budapest, Hungary 1111*
[2]*Polymer Competence Center Leoben GmbH, Roseggerstrasse 12, Leoben, Austria 8700*

Received 18 June 2010; accepted 1 September 2010
DOI 10.1002/app.33341
Published online 23 December 2010 in Wiley Online Library (wileyonlinelibrary.com).

ABSTRACT: Biodegradable polymers, blends, and composites are often investigated during tissue engineering studies, but their fracture properties, which are important mechanical engineering characteristics, are often disregarded or wrongly treated. In this study, essential work of fracture tests were performed on calcium carbonate filled poly(ε-caprolactone), a very ductile polymer, to determine the effects of different filler shapes (calcite spheres and aragonite whiskers), sizes, and contents on the fracture parameters. Increasing the filler content caused stability problems during crack propagation, and this influenced the self-similarity of the load–displacement response and resulted in the yielding point being missed. Moreover, the yielding-related essential work of fracture and the energy dissipating during yielding were found to be almost independent of the filler content and thus could be indicators of matrix–filler adhesion. A shape effect of aragonite whiskers appeared during stable crack propagation; the motion of the particles and the friction on their surface slightly increased the dissipated energy quantum and resulted in a more oriented molecular structure. © 2010 Wiley Periodicals, Inc. J Appl Polym Sci 120: 2587–2595, 2011

Key words: biodegradable; composites; fracture; polyesters; toughness

INTRODUCTION

In mechanical engineering applications, not only the strength and modulus but also the toughness of the material should be emphasized because different stress fields and material inhomogeneities can result in crack formation as well as propagation. The toughness is important with respect to the product's endurance, too. Cracks in the product can result in faster failure and usually at lower stresses than the yield strength. During tissue engineering experiments, however, the characterization of these material properties is often disregarded. Although tissue implants sustain repeated loads, most of the known literature concerns only quasi-static mechanical properties.

The consequences of toughness in bone tissue engineering become clear when we consider it from a medical point of view. In a clinical study, Bergsma et al.[1] found encapsulated, partially degraded poly(l-lactide) fragments in patients even 6 years after implantation. These fragments caused postoperative pain and inflammation. In another experiment, Eufinger et al.[2] examined cranial implants in sheep *in vivo*. The graded cranial implants consisted of poly(l-lactide), poly(d,l-lactide), and different calcium salts. They found that after 12 months, the implants started to break into fragments, and after 18 months, small scraps (10–30 μm) remained embedded in newly grown bone. In a recent review, Schafer and Werner[3] analyzed the relationship between the wound-healing process and the development of cancer. The authors stated that a multitude of clinical observations had shown that cancer is frequently a result of chronic inflammation in different tissues or organs. They said that the reactive molecules emerging during the inflammatory phase can directly damage DNA. Therefore, in chronically inflamed tissues, the frequency of malignant transformation increases. As a result, a major challenge in tissue engineering is to reduce implant fragmentation and thus chronic inflammation.

To reduce fragmentation, the degradation mechanism of the implant should be surface erosion, or the implant should maintain high toughness until the end of the healing process.

It is well known that polylactides (PLAs) possess low toughness but high strength and high modulus.

Correspondence to: F. Tuba (tuba@pt.bme.hu).
Contract grant sponsor: New Hungary Development Plan; contract grant number: TÁMOP-4.2.1/B-09/1/KMR-2010-0002.

On the other hand, poly(ε-caprolactone) (PCL) is a semicrystalline polymer and has a low melting point (55–65°C) and glass-transition temperature (−60°C); this results in high toughness but relatively low strength at body temperature. PCL and its copolymers have high potential in skin and blood vessel replacements.[4] However, numerous research groups have tried to widen the range of applications and have attempted to improve its strength and modulus by mixing it with different biocompatible polymers[5–7] or using it as a matrix for composites and nanocomposites.[8]

Because PCL is a very ductile material (its elongation at break is >700%[9]), its fracture toughness cannot be characterized by linear elastic fracture mechanics. For high deformations, elastic–plastic fracture mechanics is applicable. The most common elastic–plastic fracture mechanics methods in the literature are the J-integral and the essential work of fracture (EWF). Although the J-integral is theoretically well described, it does not treat the viscoelastic behavior of polymers and only holds if the fracture process zone is relatively small. Moreover, the measurements are both time-consuming and difficult. The EWF concept is mostly based on semiempirical considerations, but several studies have shown its relevance for polymers.[10–17]

PCL also has good biocompatibility comparable to that of tissue-culture polystyrene.[9] It is biodegradable, but its degradation rate is quite slow; consequently, it is an adequate candidate for prolonged medical applications such as bone tissue engineering. In our previous work, we proved the positive effect of the calcium carbonate salts on biocompatibility, and we also analyzed the quasi-static mechanical properties (tensile and compressive) of calcite- and aragonite-filled PCL.[9] Because scaffolds are mostly porous structures, the material discontinuities represent a real problem; it is also worthwhile to analyze the properties of precracked specimens. Additionally, during degradation, the amorphous parts deteriorate faster, and this can lead to craze formation and finally to implant fragmentation as well.[2]

Generally, concepts of linear or nonlinear elastic fracture mechanics are used because of their relative simplicity. However, these methods do not represent the viscoelastic nature of polymers because they assume reversible behavior. They can be used only under certain conditions to compare different polymers and to describe their nature until crack initiation. Originally, the EWF method was also developed for ductile metals to describe their fracture properties until crack initiation and during stable crack propagation. However, under the following limitations and application conditions, the EWF method is also valid for polymers:

- The full ligament yields before stable crack propagation.

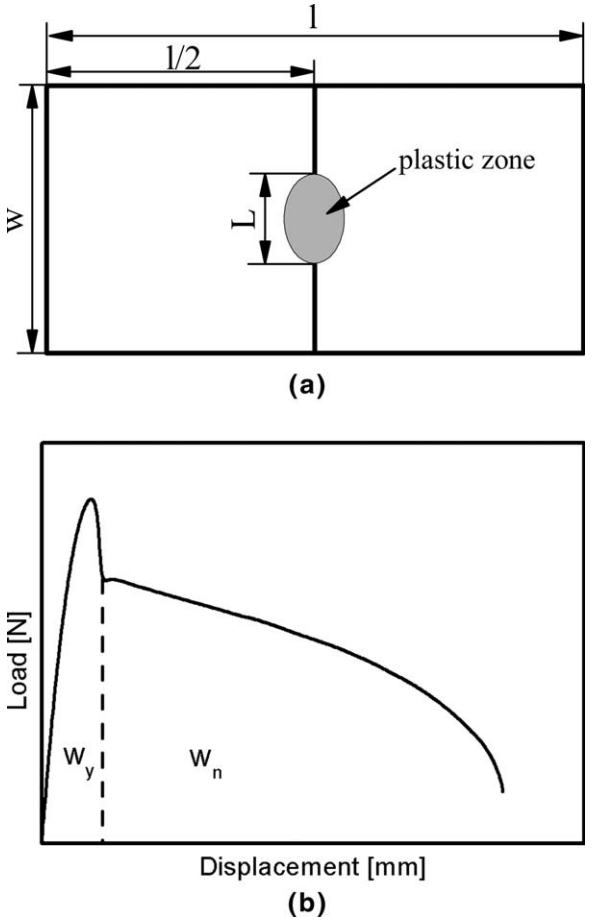

Figure 1 (a) Sample dimensions of the DEN-T specimen and (b) partitioning of the load–displacement response.

- The load–displacement curves are self-similar.
- The ligament length (L) is at least 3 times greater than specimen thickness t ($L \geq 3t$) to prevent a plane strain–stress state.[16]
- L is at most a third of specimen width w ($w/3 > L$). In this case, the fracture process does not reach the specimen edges.
- All the specimens satisfy the stress criteria, that is, $0.9\sigma_m < \sigma_{max} < 1.1\sigma_m$, where $\sigma_{max} = F_y/Lt$ is the yield stress, F_y is the maximum force at yield, and σ_m is the mean of σ_{max}.

Figure 1(b) shows a characteristic response of a double-edge notched tensile (DEN-T) specimen. If the test meets all the previously specified requirements, the total work of fracture (W_f) can be calculated with the following equation:

$$W_f = \int_0^s F(s)\,ds, \tag{1}$$

where $F(s)$ is the load and s is the displacement. W_f can be further divided into the work spent for the

generation of new surfaces (W_e) and the work related to the dissipation mechanisms (W_p). W_e corresponds to a plane and is therefore a function of area Lt, whereas W_p dissipates in volume L^2t. Accordingly, (eq. 1) can be specified and rewritten as follows:

$$w_f = w_e + \beta w_p L, \tag{2}$$

where $w_f = W_f/Lt$ is the total specific work of fracture, $w_e = W_e/Lt$ is the specific essential work of fracture, $w_p = W_p/L^2t$ is the specific plastic work of fracture, and β is a geometry-dependent correction factor. The linear regression of the plot of w_f versus L results in w_e and βw_p. According to the literature, EWF parameters depend on the molecular weight,[13,14] deformation rate,[12] temperature,[15] loading mode, thermal annealing,[17] and aging.[10] Karger-Kocsis and coworkers[12–14] proposed the splitting of the EWF response [Fig. 1(b)] when the yielding and necking of a DEN-T specimen occur. According to their model, the required W_f term can be separated into two terms: (1) the work required to yield the specimen (W_y) and (2) the work required to tear the necked ligament area (W_n). Formally, eq. (2) can be rewritten as follows:

$$\begin{aligned} w_f &= w_e + \beta w_p L = w_y + w_n \\ &= w_{e,y} + \beta_y w_{p,y} L + w_{e,n} + \beta_n w_{p,n} L, \end{aligned} \tag{3}$$

where w_n is the specific necking-related work of fracture, w_y is the specific yielding-related work of fracture, $w_{e,y}$ is the specific yielding-related essential work of fracture, $w_{e,n}$ is the specific necking-related essential work of fracture, $w_{p,y}$ is the energy dissipated during yielding, and $w_{p,n}$ is the work dissipated during tearing. β_y and β_n are geometry factors related to the shape of the plastic zone during the yielding and necking stages, respectively.[16] The advantage of this partitioning is that $w_{e,y}$ seems to be independent of the molecular weight[13,14] and deformation rate;[12] both parameters influence only the tearing-related parameters. On the other hand, $w_{e,y}$ and $\beta_n w_{p,n}$ seem to be suitable for predicting the effect of physical aging.[10]

The aim of this study was to reveal the effects of different amounts and shapes of fillers on the fracture properties and EWF parameters of biodegradable PCL. Additionally, the adaptability limitations of this method were analyzed in these materials.

EXPERIMENTAL

Materials

For the measurements, PCL (Perstorp UK Ltd., Warrington, UK) with a nominal number-average molecular weight of 80 kDa and PLA (Natureworks LLC, Minnetonka, MN) with a nominal number-average molecular weight of 100 kDa were used. Before processing, each polymer was dried at 40°C over a day.

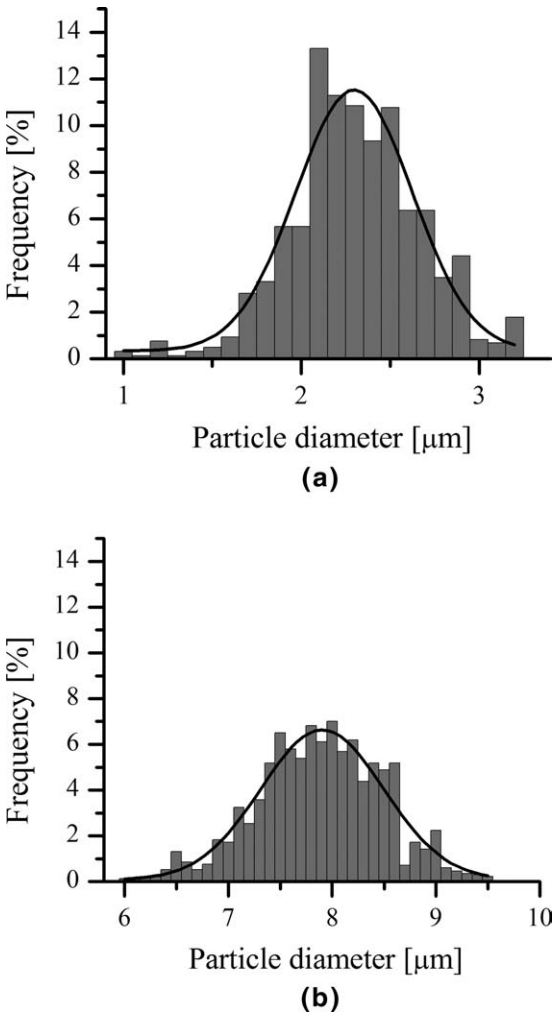

Figure 2 Particle size distribution of (a) the calcite filler and (b) the aragonite filler (determined by image analysis).

Calcium carbonate was used in two crystal forms. The calcite filler was purchased from Sigma–Aldrich, Inc (St. Louis, MO). The median diameter of the spherical particles was determined by scanning electron microscopy (SEM) to be 2.3 μm [Fig. 2(a)], whereas the specific surface area was 5.7 m^2/g. Aragonite whiskers were kindly supplied by the Bioceramic Department of the Institute of Glass and Ceramics (Warsaw, Poland). The median diameter of the crystals was 7.9 μm [Fig. 2(b)], and the length varied from 30 to 50 μm. The specific surface area of this filler was 1.4 m^2/g. The major differences in the properties originated from the different particle geometries and lattice structures. Calcite has a rhombohedral lattice and a density of 2.71 g/cm^3. Aragonite has an orthorhombic lattice, and its density is 2.95

g/cm^3. It is noteworthy that the naturally stable form of calcium carbonate is calcite; therefore, the precipitation method was applied to obtain aragonite whiskers.

Methods

The specific surface area of the filler was determined with an Autosorb 1 apparatus (Quantachrome, Boynton Beach, FL). Nitrogen was used as an adsorbent, and the measurements were carried out at the temperature of liquid nitrogen ($\sim$ 77 K). The samples were degassed in a 10^{-3} Pa vacuum for 24 h, and then a part of the adsorption isotherm of N_2 was measured on the filler. The monomolecular capacity was determined from the linearized form of the equation describing the multilayer, Brunauer–Emmett–Teller type II adsorption of a gas on the filler surface. The monomolecular capacity is the amount of the adsorptive needed to cover a unit surface with a monolayer. The linearized Brunauer–Emmett–Teller equation could be used in the relative pressure range of 0.05–0.35; five points were measured. The linear fit was very good; the correlation coefficient was always greater than 0.999. The specific surface area could be calculated from the monomolecular capacity and from the area occupied by a single gas molecule. In the calculations, the latter value was considered to be 0.162 nm^2.

To obtain materials with precise compositions (i.e., a filler concentration of 10, 30, or 50 wt %), an analytical balance (Ohaus Explorer, Ohaus Corp, Pine Brook, NJ) with an accuracy of $\pm$0.1 mg was applied to measure the materials before processing. The materials were blended in a Brabender PL2000 (Brabender GmbH, Duisburg, Germany) internal mixer at 100°C and 25 rpm for 15 min. Subsequently, sheets with a thickness of 1 mm were hot-pressed at 100°C and 5 MPa with a Collin P-200E (Dr. Collin GmbH, Ebersberg, Germany) compression-molding machine, and this was followed by a water cooling of 10°C/min.

The EWF study was performed on DEN-T specimens. Samples with a width of 40 mm and a length of 60 mm (gauge length = 40 mm) were machined from the sheets. L was set to 4, 6, 8, 10, or 12 mm. The notches were prepared with aligned razor blades, and at each ligament, at least three specimens were tested. The load–displacement curves were recorded under the ambient conditions (25°C and 48% relative humidity) with a Zwick (Zwick GmbH, Ulm, Germany) Z020 universal testing machine with a crosshead speed of 10 mm/min.

SEM images of the surfaces of the fillers and specimens were taken with a JEOL 6380LA (JEOL Ltd., Tokyo, Japan) instrument. Before the test, a JEOL JFC-1200 fine coater was used to form a thin layer of gold on the samples. A magnification range of 50–4000× was applied. The geometrical data for the fillers were determined from microscopic measurements.

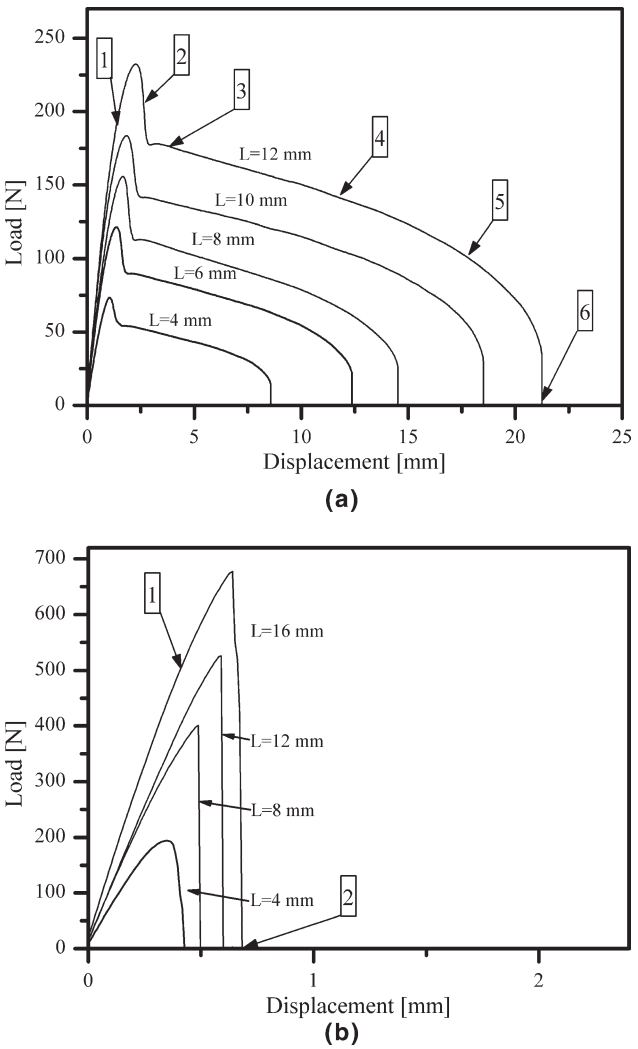

Figure 3 Characteristic load–displacement curves of (a) PCL and (b) PLA (DEN-T specimens with a crosshead speed of 10 mm/min). The numbers in squares indicate the stages of the fracture process in Figure 4.

Thermal analysis, differential scanning calorimetry (DSC), was carried out with a PerkinElmer DSC2 (PerkinElmer Inc., Waltham, MA) between 25 and 100°C at a heating rate of 5°C/min. The results were evaluated according to the ISO 11357-3 standard.

RESULTS AND DISCUSSION

Application limit

In the known literature, the conditions of EWF testing are sometimes disregarded. Figures 3 and 4 show the major differences between a ductile polymer (PCL) and a relatively rigid polymer (PLA).

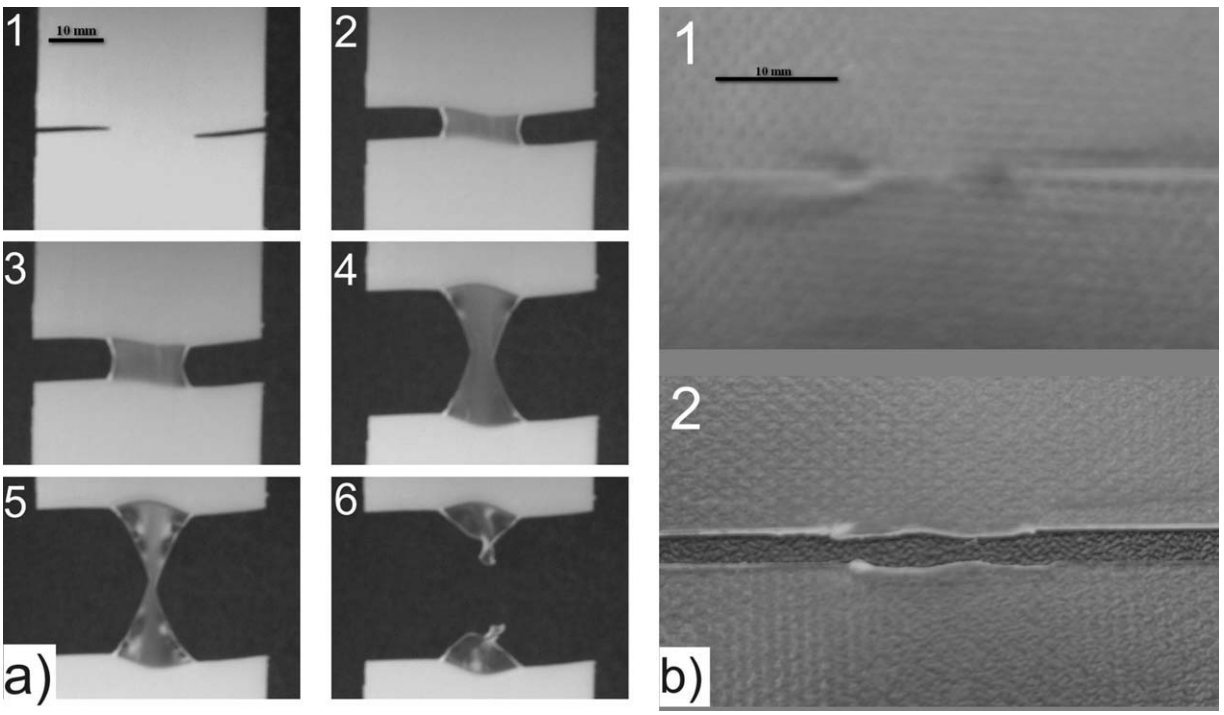

Figure 4 Photographs of the fracture process of (a) PCL and (b) PLA specimens.

Although self-similarity showed up in both cases for wide ligament ranges, ligament yielding and stable crack growth did not occur in PLA specimens. This resulted in a negative slope after linear regression, which is one of the indicators that the EWF technique is not adaptable.

The major problem with fillers is that increases in the particle content may also result in the slope decreasing[11] and the yielding point being missed. Moreover, when the yielding is suppressed, curve partitioning should not be used either.

In this study, a filler concentration of 10 wt % did not affect the yielding behavior of the materials significantly. With increasing filler content, the self-similarity of load–displacement curves deteriorated. This was especially true for calcite-reinforced polymers, for which the polymer–filler and filler–filler interactions were stronger [Fig. 5(d)]. The larger deviations during crack propagation with higher filler contents and higher L values were attributed to aggregation and particle-related material inhomogeneities. Figure 5 also indicates the lower margin of the curve-partitioning EWF approach. With a 30 wt % filler concentration, this extremity was at $L = 4$ mm, whereas with a 50 wt % filler concentration, it increased to 8 mm. The basis for this was the decreasing relative polymer content in the ligament. In these cases, the yielding became less observable, and the yielding and necking processes were hardly severable; thus, the associated results should be treated with reservation.

Determination of the EWF parameters

Before linear regression, the stress criteria were analyzed for each material. The results are summarized in Table I. Specimens that did not fulfill the aforementioned criterion were left out from further analysis.

The higher yield strength of the calcite-filled materials suggested better adhesion between calcite and PCL in comparison with the aragonite-reinforced ones. This phenomenon could be related either to the different specific surface areas or to the different surface properties.

The linear regression fitted well in all cases; the coefficients were high (>0.95). Figure 6 also indicates that w_n and thus w_f scattered more than w_y. This can be explained by the inhomogeneities of the material and different local instabilities at high deformations. These inhomogeneities and instabilities could have arisen from the different stress fields and various cavitational mechanisms around the particles.[18] Until yielding, these effects were smaller; thus, the use of w_y to describe the properties of filled materials could be beneficial.

With high filler contents (Fig. 7), especially for calcite-reinforced composites, the results for samples with $L = 12$ mm deviated from linearity. At higher values of L, higher stresses were required to initiate the plastic flow, so yielding sometimes occurred not only in the cracked region but also in its surroundings. The resultant crack kinking caused local material instabilities and thus probably stress field

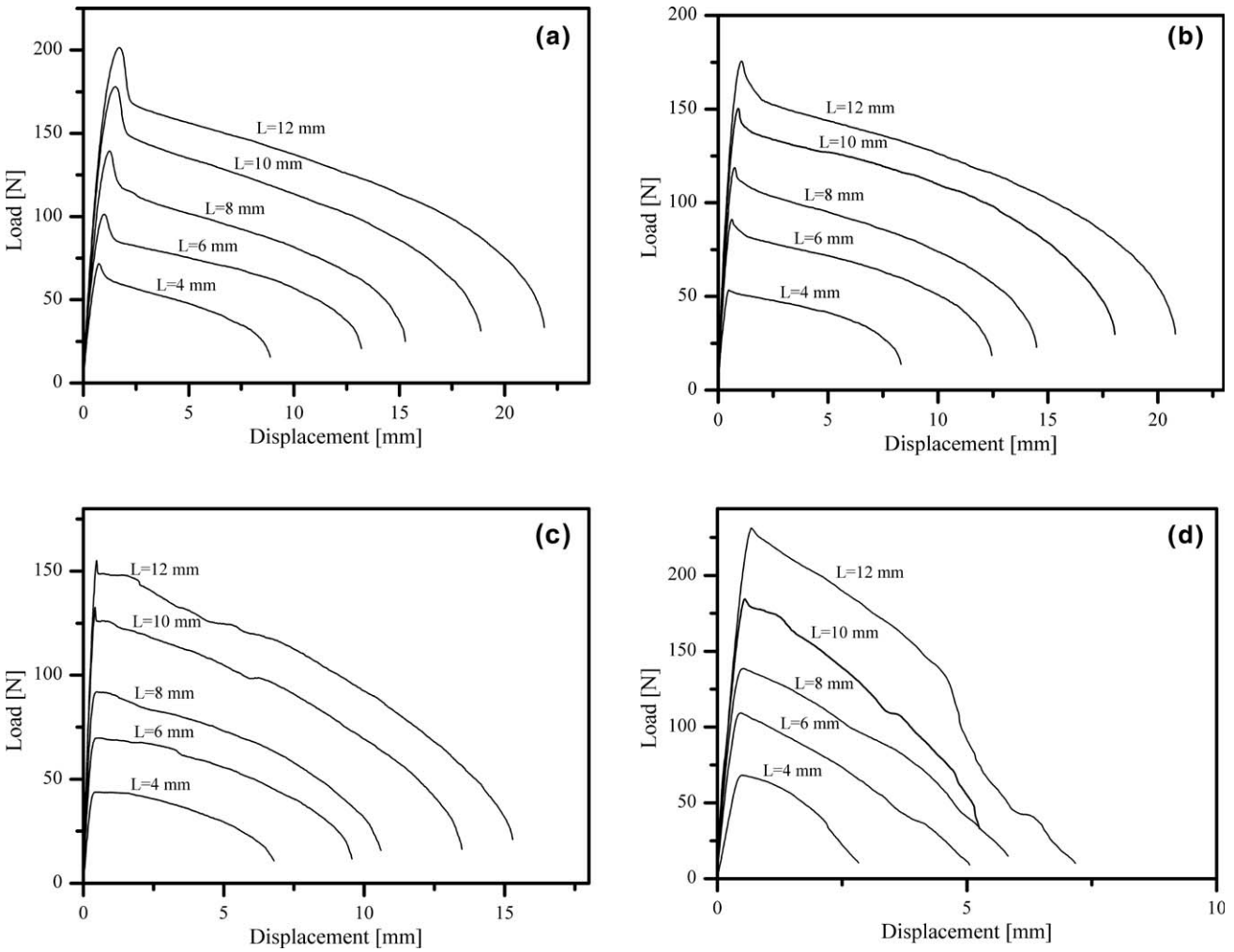

Figure 5 Load–displacement curves of samples with (a) 10 wt % aragonite, (b) 30 wt % aragonite, (c) 50 wt % aragonite, or (d) 50 wt % calcite (DEN-T specimens with a crosshead speed of 10 mm/min).

changes. The pure mode I load turned into a mixed mode I/mode II load. It is well known that materials possess lower shear resistance than tensile resistance, so the related specific work also decreases after small changes in the load mode. Hence, the results showing this kind of deviation were left out of further analysis and linear regression.

Figure 8 summarizes the attained EWF properties. The yielding-related terms ($w_{e,y}$) remained small and nearly constant, and this suggested relatively poor adhesion between the matrix and filler materials. However, the only exception (90/10 PCL/calcite) and the overall better properties of calcite-filled samples underlined the former assumption of better interactions between PCL and calcite spheres before yielding. As also mentioned earlier, filler aggregation (Fig. 9) suppressed this effect at higher particle contents.

Contradictorily, $w_{e,n}$ increased. The $w_{e,n}$ parameter doubled in the cases of 90/10 PCL/calcite, 90/10 PCL/aragonite, and 70/30 PCL/aragonite in comparison with neat PCL. This means that the formation of new fracture surfaces required more energy during crack propagation. This could be associated with the debonding processes between the filler and the matrix material and with the local orientation of the polymer chains around the particles. The fillers with high moduli and strength retarded the plastic

TABLE I
Mean Values of Yield Stress and Stress Criteria for the Analyzed Materials

	PCL	10 wt % calcite	30 wt % calcite	50 wt % calcite	10 wt % aragonite	30 wt % aragonite	50 wt % aragonite
σ_m (MPa)	19.20 ± 0.86	19.21 ± 1.09	19.00 ± 1.18	18.15 ± 0.95	17.58 ± 0.74	14.94 ± 0.58	12.27 ± 0.86
0.9–1.1σ_m (MPa)	17.28–21.12	17.29–21.14	17.10–20.89	16.34–19.97	15.82–19.34	13.45–16.44	11.04–13.50

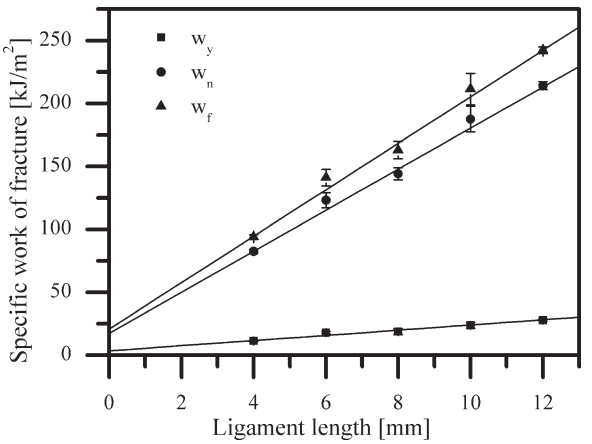

Figure 6 w_f and its contributing terms (w_y and w_n) as functions of L for PCL specimens.

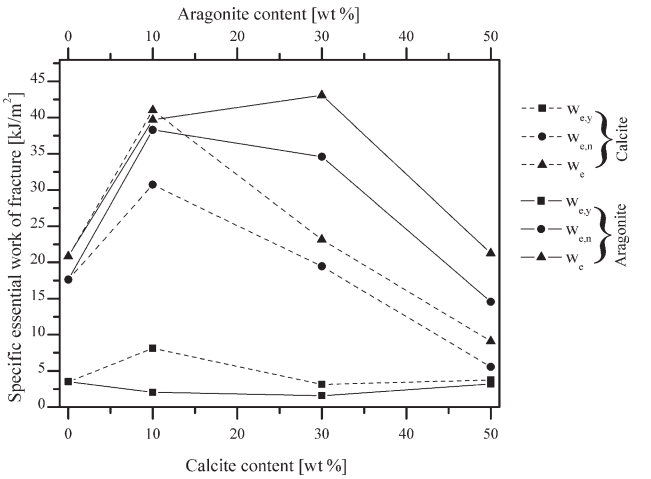

Figure 8 w_e, $w_{e,y}$, and $w_{e,n}$ for the filled materials.

flow until there was adhesion between the matrix and filler ($w_{e,y}$). Subsequently, after debonding, the orientation of molecules started. Because of the work-hardening effects in PCL, this structure became stronger, and more energy was required to form new crack surfaces (increasing $w_{e,n}$).

Figures 8 and 10 show that $w_{e,y}$ and $\beta w_{p,y}$ were independent of the filler content. The only exception was again 90/10 PCL/calcite; this suggests that these parameters are indicators of filler–matrix adhesion. In this study, when the polymer–filler adhesion was quite poor, these parameters exhibited matrix properties.

To underline the matrix domination of composites and the filler independence of $w_{e,y}$ and $\beta w_{p,y}$, DSC measurements were carried out. The results are listed in Table II and indicate that the incorporation of calcium carbonate fillers did not affect the crystallinity significantly. This observation contrasts with the results of Baji et al.,[19] who found that hydroxyapatite filling slightly increased the crystallinity of PCL.

Because the failure mode and the dimensions of the plastic zone were similar in each material, the

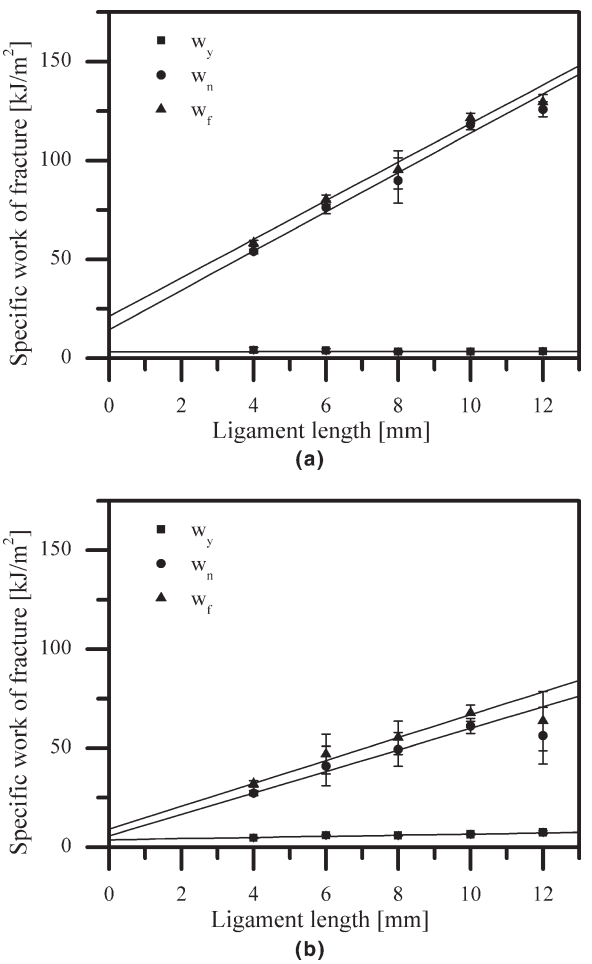

Figure 7 w_f and its contributing terms (w_y and w_n) as functions of L with (a) 50 wt % aragonite or (b) 50 wt % calcite.

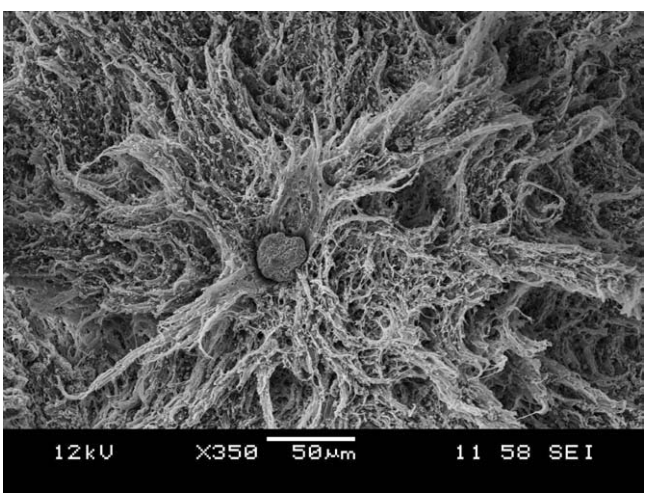

Figure 9 Aggregate found in the 50 wt % calcite reinforced blend (SEM picture).

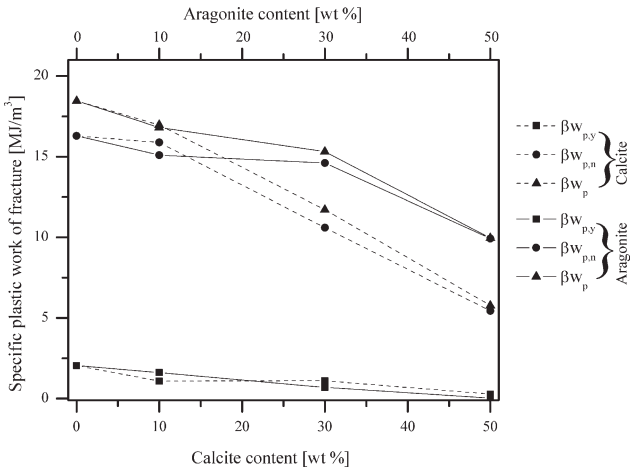

Figure 10 βw_p, $\beta w_{p,y}$, and $\beta w_{p,n}$ for the filled materials.

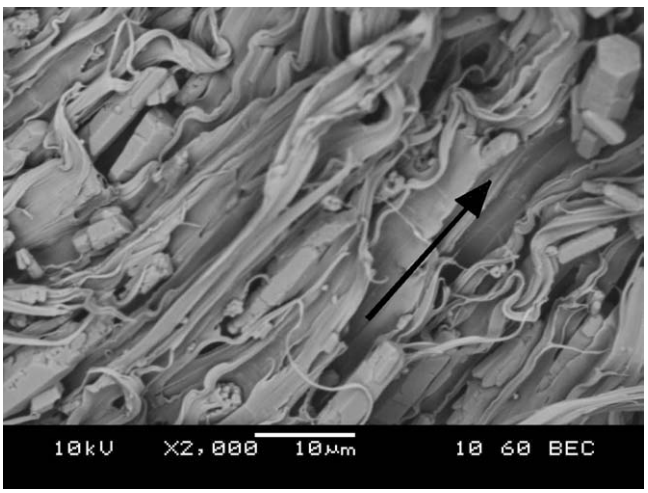

Figure 11 Aragonite whiskers oriented parallel to the loading direction (arrow) in a sample with 50 wt % aragonite (SEM picture).

obtained βw_p values were comparable. The overall plastic work of fracture (Fig. 10) decreased with increasing filler content because the rigid particles with high moduli did not take part in the plastic flow and viscoelastic energy dissipation. Calcite particles behaved as spherical voids (cavitation followed by the collapse of the cavitated structure), and the energy dissipating during necking decreased linearly with the weight fraction; thus, they did not interact with the polymer matrix significantly.

On the other hand, aragonite whiskers turned in the load direction (Fig. 11), and the friction during the particle motion and plastic flow resulted in higher specific energy values. Additionally, as mentioned earlier, during this slow motion, the PCL molecules became oriented between the cavities, and this oriented structure resulted in higher toughness and caused a slower collapse of cavities.

Figures 8 and 10 also suggest that a low reinforcing material content hinders crack initiation in the mode I load through the local orientation of macromolecules. Thus, the work required for the formation of new crack surfaces (w_e) increases in tough polymers. However, as the filler fraction increases, the aggregation processes demolish the properties of these materials in the crack propagation phase (βw_p). Tough materials should have high w_e and βw_p values. If βw_p is low, the material is rigid and cannot withstand the propagation of a previously formed crack. On the other hand, low w_e values usually result in low tensile strength, modulus, and resistance to crack initiation.

CONCLUSIONS

In this study, the fracture mechanical properties of PCL reinforced by two forms of calcium carbonate (spherical calcite and needlelike aragonite) were analyzed with the EWF method. These materials are important in tissue engineering, and they could be beneficial in other biodegradable applications.

The EWF method was originally developed for ductile metals but later was used for ductile polymers as well. There are, however, several limitations that the polymers have to meet during the tests. If self-similarity of load–displacement curves does not exist, the linear regression of data and thus the EWF method are unsuitable. The crack growth has to be

TABLE II
Thermal Properties of PCL and Its Composites with Calcite and Aragonite

	PCL	10 wt % calcite	30 wt % calcite	50 wt % calcite	10 wt % aragonite	30 wt % aragonite	50 wt % aragonite
$T_{m,p}$ (°C)	61.4	61.4	61.4	61.4	61.8	60.9	60.1
ΔT_m (°C)	24	24	24	23	24	23	24
ΔH_m (J/g)[a]	79.6	81.9	79.0	77.9	80.3	76.6	77.6
X (%)[b]	55.9	57.5	55.4	54.6	56.3	53.8	54.5

ΔH_m = melting enthalpy; ΔT_m = melting temperature range; $T_{m,p}$ = peak temperature of melting; X = crystallinity.
[a] Calculated from the nominal composition.
[b] Estimated with 142.5 J/g as the heat of fusion for the 100% crystalline material (from Crescenzi et al.[20]).

stable; otherwise, the slope of regression has a negative value. The major problem with fillers is that at high deformations, they mostly behave as voids, inhomogeneities, and thus crack-initiation points. They can ruin the self-similarity and cause unstable crack propagation.

We analyzed filler concentrations of 10, 30, and 50 wt % and found that only high calcite contents demolished the self-similarity significantly (because of the smaller particles and better adhesion between calcite and PCL versus aragonite and PCL), but stable crack propagation was present in all samples. The increasing filler content, however, suppressed the yielding, so the partitioning of the load–displacement response at lower values of L was conjectural. We also found that the effect of material inhomogeneities before yielding was smaller, so w_y could be used to describe general material characteristics. Additionally, $w_{e,y}$ and $w_{p,y}$ were almost independent of the reinforcement content and thus could be indicators of matrix–filler adhesion as well as matrix characteristics when the adhesion is poor. DSC measurements also underlined that the polymer morphology does not depend on fillers because the crystallinity of PCL was influenced by neither aragonite nor calcite. The effect of aggregation manifested in $w_{e,n}$, which dropped significantly with increasing filler content. After yielding, as expected, the fillers did not interact with the polymer significantly, but the turning motion of aragonite whiskers and the friction on their surface resulted in slightly increased energy dissipation during plastic flow. Finally, we also observed that with long ligaments ($L = 12$ mm), the results deviated from linearity, and this suggested changes in the stress field (from the pure mode I load to a mixed mode I/mode II load).

The authors are indebted to Tamás Bárány (Budapest University of Technology and Economics, Budapest, Hungary) for his help with the EWF tests and to Zbigniew Jaegermann (Institute of Glass and Ceramics, Warsaw, Poland) for the preparation of aragonite. This work is connected to the scientific program of the project entitled "Development of Quality-Oriented and Harmonized R+D+I Strategy and Functional Model at BME."

References

1. Bergsma, J. E.; deBruijn, W. C.; Rozema, F. R.; Bos, R. R. M.; Boering, G. Biomaterials 1995, 16, 25.
2. Eufinger, H.; Rasche, C.; Lehmbrock, J.; Wehmöller, M.; Weihe, S.; Schmitz, I.; Schiller, C.; Epple, M. Biomaterials 2007, 28, 475.
3. Schafer, M.; Werner, S. Nat Rev Mol Cell Biol 2008, 9, 628.
4. Lipik, V. T.; Widjaja, L. K.; Liow, S. S.; Venkatraman, S. S.; Abadie, M. J. M. Express Polym Lett 2010, 4, 32.
5. Zhou, Z.; Huang, H.; Xu, P.; Fan, L.; Yu, J.; Huang, J. J Appl Polym Sci 2009, 112, 692.
6. Vilay, V.; Mariatti, M.; Ahmad, Z.; Pasomsouk, K.; Todo, M. J Appl Polym Sci 2009, 114, 1784.
7. Simöes, C. L.; Viana, J. C.; Cunha, A. M. J Appl Polym Sci 2009, 112, 345.
8. Kotela, I.; Podporska, J.; Soltysiak, E.; Konsztowicz, K. J.; Blazewicz, M. Ceram Int 2009, 35, 2475.
9. Oláh, L.; Tuba, F. Macromol Symp, to appear.
10. Bárány, T.; Ronkay, F.; Karger-Kocsis, J.; Czigány, T. Int J Fract 2005, 135, 251.
11. Gong, G.; Xie, B.-H.; Yang, W.; Li, Z.-M.; Zhang, W.-Q.; Yang, M.-B. Polym Test 2005, 24, 410.
12. Karger-Kocsis, J.; Ferrer-Balas, D. Polym Bull 2001, 46, 507.
13. Karger-Kocsis, J.; Moskala, E. Polym Bull 1997, 39, 503.
14. Karger-Kocsis, J.; Moskala, E. J. Polymer 2000, 41, 6301.
15. Kuno, T.; Yamagishi, Y.; Kawamura, T.; Nitta, K. Express Polym Lett 2008, 2, 404.
16. Mouzakis, D. E.; Karger-Kocsis, J.; Moskala, E. J. J Mater Sci Lett 2000, 19, 1615.
17. Wallner, G. M.; Major, Z.; Maier, G. A.; Lang, R. W. Polym Test 2008, 27, 392.
18. Jerabek, M.; Major, Z.; Renner, K.; Móczó, J.; Pukánszky, B.; Lang, R. W. Polymer 2010, 51, 2040.
19. Baji, A.; Wong, S.-C.; Liu, T.; Li, T.; Srivatsan, T. S. J Biomed Mater Res B 2007, 81, 343.
20. Crescenzi, V.; Manzini, G.; Calzolari, G.; Borri, C. Eur Polym J 1972, 8, 449.